Optimization of Engine Torque Management Under Uncertainty for Vehicle Driveline Clunk Using Time-Dependent Metamodels

Daniel Wehrwein
e-mail: daniel.wehrwein@gm.com

Zissimos P. Mourelatos[1]
e-mail: mourelat@oakland.edu

Department of Mechanical Engineering,
Oakland University,
Rochester, MI 48309

Quality and performance are two important customer requirements in vehicle design. Driveline clunk negatively affects the perceived quality and must be minimized. This can be achieved using engine torque management, which is part of engine calibration. During a tip-in event, the engine torque rate of rise is limited until all the driveline lash is taken up. The engine torque rate of rise can negatively affect the vehicle throttle response, which determines performance. The engine torque management must be therefore balanced against throttle response. In practice, the engine torque rate of rise is calibrated manually. This article describes an analytical methodology for calibrating the engine torque considering uncertainty, in order to minimize clunk, while still meeting throttle response constraints. A set of predetermined engine torque profiles are considered, which span the practical range of interest. The transmission turbine speed is calculated for each profile using a bond graph vehicle model. Clunk is quantified by the magnitude of the turbine speed spike. Using the engine torque profiles and the corresponding turbine speed responses, a time-dependent metamodel is created using principal component analysis and kriging. The metamodel predicts the turbine speed response due to any engine torque profile and is used in deterministic and reliability-based optimizations to minimize clunk. Compared with commonly used production calibration, the clunk disturbance is reduced substantially without greatly affecting the vehicle throttle response. [DOI: 10.1115/1.3086788]

1 Introduction

To be competitive, automotive manufacturers strive for dependable and high quality vehicles. The definition of quality has evolved from strictly functionality and durability to pleasability. Noise, vibration, and harshness (NVH) issues, such as squeaks, rattles, wind noise, and gear whine, are "unwanted" noises, which are perceived as poor quality, although they do not affect the vehicle functionality. Driveline clunk is also a perceived NVH quality issue.

Driveline clunk (or clonk in Europe) is a phenomenon that occurs while the drivetrain gear transitions from the drive to the coast side of the gear teeth or vice versa. As shown in Fig. 1, a finite amount of lash is inherent in every gear set by design. If there is no lash, the gear set cannot rotate. In the presence of lash, the gear teeth travel through a lash zone. While in the lash zone, the gear accelerates until it contacts the drive side of the gear tooth at the end of the lash zone. Clunk occurs when the faster moving gear set collides with the slower moving gear set. The momentum of the driveline collision causes the vehicle to jerk and, in some cases, results in an audible metallic sound. It can also affect gear durability and driveline reliability. The jerk and the sound associated with clunk are perceived by the customer as either a problem with the vehicle or as a low quality attribute. Because of the quality degradation and the durability concern, automotive manufacturers try to eliminate, or at least reduce the intensity of the clunk phenomenon.

Driveline clunk can occur under different driving conditions such as transmission ratio shifts, parking lot shifts from drive to reverse, ABS maneuvers, and throttle application and release. It can also be observed in manual transmission applications during clutch engagement and disengagement. Although clunk occurs during various driving conditions, the focus of this study is on its occurrence during throttle application maneuvers. This is commonly referred to as "tip-in clunk" because it happens when the driver tips in on the throttle pedal. Tip-in clunk occurs only when there is a transition from negative to positive torque in the driveline. The gear sets are on the coast side of the gear teeth while the driveline torque is negative, and on the drive side of the gear teeth when the driveline torque is positive. Tip-in clunk has also been referred to as throttle-on clunk, fore-aft tactile disturbance, impact induced vibration, and sudden throttle demand clunk.

In order to reduce its severity, the automotive industry uses engine torque management to reduce the net torque on the driving gear as it transitions through the lash zone. This reduces the impact intensity when the driving gear collides with the driven gear. A feed-forward engine torque controller is the current state-of-the-art in automotive design, and is used in this work. More sophisticated engine torque controllers, which estimate the current lash state in the drivetrain have also been considered [1–3]. Although these controllers are promising, they must be further developed.

Reducing engine torque will reduce clunk, but it will also reduce the vehicle's acceleration performance. Reducing clunk with a minimal impact on vehicle performance requires a controller to shape the engine output torque as needed, without intervening when the driveline is not crossing the lash zone. This requires precise calibration. If the engine torque rises too rapidly, it causes a large clunk disturbance. If it rises slowly however, it results in a large delay between the driver's request and the throttle response. This trade-off can be resolved by optimizing the engine torque shape.

[1]Corresponding author.

Contributed by the Design Automation Committee of ASME for publication in the JOURNAL OF MECHANICAL DESIGN. Manuscript received February 4, 2008; final manuscript received January 5, 2009; published online April 3, 2009. Review conducted by Shapour Azarm. Paper presented at the ASME 2008 Design Engineering Technical Conferences and Computers and Information in Engineering Conference (DETC2008), Brooklyn, NY, July 6–August 3, 2008.

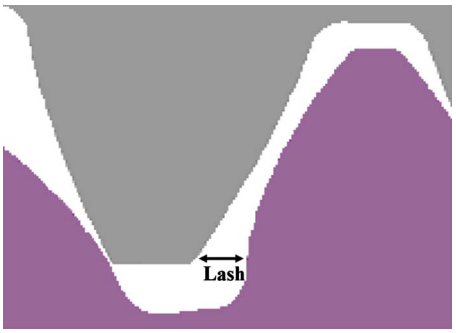

Fig. 1 Illustration of gear set lash

In this article, the shape of the engine torque is optimized to minimize clunk while meeting a throttle response target. In doing so, it is possible however, to have other adverse effects, such as vehicle shuffle [4], which is caused by a rapid rise in engine torque. The proposed methodology can also address vehicle shuffle by using an additional constraint in the optimization problem in Secs. 6 and 7. We chose not to consider vehicle shuffle, however, because it occurs after the clunk event, and is usually addressed with a different torque control strategy.

A set of time-dependent engine torque profiles are used as input in a vehicle dynamic model (see Sec. 3), and the resulting time-dependent transmission turbine speed profile is calculated for each engine torque. Principal component analysis (PCA) is then used to build time-dependent surrogate models (metamodels) of the engine torque input and the corresponding turbine speed output, providing an accurate and efficient input-output relationship, which allows us to use optimization. The throttle response is quantified by the time it takes for the engine torque to reach a specified value. The clunk event is quantified by the magnitude of the turbine speed spike during a tip-in because it represents the speed of the colliding gear set. The clunk severity increases with an increasing magnitude of the turbine speed spike.

To our knowledge, this is the first study using time-dependent metamodeling and optimization to reduce the tip-in clunk disturbance. The time-dependent metamodels reproduce the time-dependent sample functions of a parametric random process.

2 Quantification of Driveline Clunk

The driveline consists of the propshaft and axle, as shown in Fig. 2. Several papers have been published on driveline clunk describing how to quantify and reduce its severity using both experimental and analytical methods [5–19].

Driveline hardware changes are proposed in Refs. [5–8], focusing on lash reduction and increased damping. As we have mentioned, lash reduction is very costly and has physical limitations. If it is reduced, clunk also reduces because the accelerating gear sets have less time to build up speed before they impact the slower moving gear sets. Even if lash is reduced to an absolute minimum however, clunk can still occur if the torque input to the driveline is not managed [14,15]. Increasing driveline damping can reduce clunk, but it also reduces the driveline efficiency and the vehicle's fuel economy because it provides resistance to the gear sets while in the lash zone, lowering the speed difference between gear sets during impact. Both of these solutions have therefore, large negative impacts.

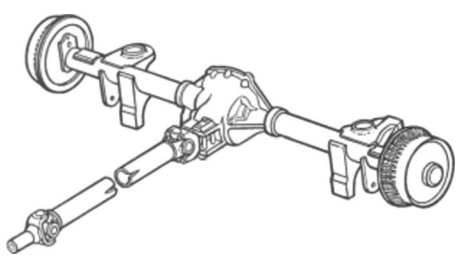

Fig. 2 Driveline schematic

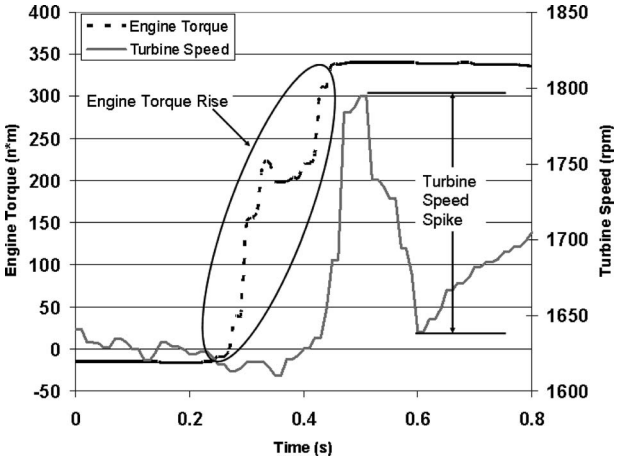

Fig. 3 Illustration of the transmission turbine speed spike during a tip-in

A parametric study in Ref. [5] showed that increasing the transmission and flywheel inertia can reduce clunk. Also compliant rubber mounts in the driveline can reduce clunk [8]. Garage shift clunk was experimentally addressed in Refs. [6,7] for a front-wheel-drive (FWD) vehicle with an automatic transmission. It was observed that a reduction in driveline lash reduces clunk, and that the clunk severity is proportional to the magnitude of the input torque.

The clunk phenomenon was studied in Refs. [9,10] for manual transmission vehicles using a torsional vibration analysis of the driveline with emphasis on the "declutch" clunk, which does not require an engine model. An experimental test rig was used in Refs. [11,12] for a rear-wheel-drive (RWD) vehicle with a manual transmission. The driveline natural frequencies and mode shapes, which contribute to the clunk, were used in Ref. [11], and possible acoustic improvements to reduce the severity of the audible clunk were considered in Ref. [12]. A relationship between clunk and shuffle was indicated in Ref. [13].

Engine torque management is a promising and cost effective way to reduce clunk [6,14–17]. It must be done optimally though, in order to avoid a negative impact on fuel economy. Most of the reported studies to reduce clunk (e.g., Refs. [14–17,6]) vary certain design variables arbitrarily and calculate, or measure, their effect on clunk. Optimization is used only in Ref. [4], where a genetic algorithm minimizes clunk by varying the flywheel inertia, driveline lash, and the clutch spring stiffness. Our proposed approach provides a unique method to determine the optimal engine torque shape to minimize the clunk without excessively sacrificing the vehicle performance.

There are no standards for quantifying tip-in clunk. Several studies have used, however, the relative speed of the colliding gears to establish a metric for clunk severity [14–16,18]. They indicate that the relative speed between gear sets is proportional to the clunk severity. The transmission turbine speed is a commonly measured signal in most automotive applications and is used to quantify clunk in this article.

As the driveline passes through the lash zone, there is very little resistance and the gears speed up rapidly. The turbine speed spikes momentarily until the gear sets collide on the other side of the lash zone. Figure 3 illustrates this phenomenon using measured engine torque and turbine speed time traces for a rear-wheel-drive light duty truck. As the driver presses the throttle pedal rapidly, the engine torque rises abruptly and the transmission turbine speed

spikes. In this article, we calculate an optimal engine torque profile under uncertainty by minimizing the magnitude of the turbine speed spike.

3 Overview of Vehicle Dynamic Model

Developing a dynamic model to simulate vehicle performance requires accurate modeling of the engine, transmission, drivetrain, and vehicle. The bond graph method [20–22] has been used in this article because of its modularity, simplicity, modeling accuracy, and graphical representation of the simulated system. It can also handle multiple disciplines, such as mechanical, electrical, and hydraulic, simultaneously. Bond graphs allowed us to develop a model for each subsystem separately and then to assemble all models, providing flexibility to improve any subsystem without having to model the entire system over. Because of its distinct modeling advantages, the bond graph method has been extensively used in vehicle dynamics [20] and powertrain analysis [21].

Bond graphing was only used for modeling. The numerical simulation was carried out using MATLAB SIMULINK. For that, an equivalent block diagram was developed based on the bond graph model. The MATLAB environment was then used for all simulations, including the deterministic and probabilistic optimizations.

Sections 3.1–3.3 give a brief description of the engine, torque converter, transmission, and driveline and vehicle models. Details can be found in Refs. [23].

3.1 Engine Model. A detailed engine dynamics model is not needed in estimating vehicle performance. Instead, the engine can be modeled as a rigid body with a lump inertia. The engine torque is estimated using a steady-state torque map obtained from dynamometer data [21,23,24]. The engine inertia and friction are lumped into a single inertia element and friction element, respectively. The lump engine inertia includes the flywheel and torque converter housing inertias. The engine speed and throttle position are fed into the torque map to obtain the torque input to the system. The latter is applied to the lump engine inertia element. Some of it is dissipated at the lump friction element, and the remaining is fed to the torque converter.

Every engine uses a torque management algorithm in the engine controller, which changes the spark timing, throttle rate, and air/fuel ratio to accomplish the desired torque level. The engine controller determines the desired spark timing, throttle position, and fuel rate using an experimentally determined internal torque model based on dynamometer data at steady-state engine conditions, where the temperature, pressure, and quality of fuel are controlled. The engine torque output is measured for varying combinations of throttle position, engine speed, and spark timing, and a simple look-up table is established.

In production however, there is an inherent engine torque variation from engine to engine. In our model, the effect of this variation is represented with a positive scalar multiplication factor called engine torque variation (ETV) factor, which is close to, but smaller than, 1. A value of 1 means that there is no variation, where a value of 0.9, for example, means that the actual engine torque is 90% of the torque reported by the engine controller.

3.2 Torque Converter and Transmission Models. The torque converter is a fluid coupling device that transfers torque from the engine to the transmission. Its model is based on steady-state dynamometer data and is used similarly to the engine model to obtain the torque ratio and converter efficiency curves. The torque ratio decreases with increasing speed ratio, and the converter efficiency increases with increasing speed ratio. Similar models exist in Refs. [20,24]. The torque converter is a hydromechanical device without a control system. Variation is due to inaccuracies in geometry or transmission fluid viscosity because of variation in the transmission operating temperature.

The torque converter model uses the speed ratio between the engine and the transmission, a measured K-factor, and the torque ratio to calculate the output torque to the transmission and the load on the engine. The K-factor indicates the torque converter efficiency. It is defined as the engine speed divided by the square root of the engine torque. The K-factor and the torque ratio can account for all variation in the torque converter model. Similarly to the engine model, the positive scalar variation factors, K-factor variation (KFV), and torque ratio variation (TRV), are used as random parameters to account for variation in the torque converter model. Both KFV and TRV are close to, but smaller than, 1. The K-factor variation is important in the driveline clunk model because the torque converter efficiency determines how much torque is dissipated in the torque converter before it gets to the transmission, and eventually to the driveline.

The transmission includes a compound planetary gear set with four forward gear ratios and one reverse. Each planetary gear set is modeled using a separate lump inertia for the sun, ring, and planetary carrier. It also includes a clutch between rotating elements, a clutch brake, and a one way roller clutch. A controller actuates each clutch mechanism for the desired gear state using current driving conditions. The gear state is determined by a shift table, which uses the vehicle speed and engine throttle position as inputs. Details are provided in Ref. [23].

3.3 Driveline and Vehicle Model. The vehicle driveline connects the transmission to the vehicle wheels. A simple two-wheel drive driveline is used consisting of a propeller shaft, a reduction gear set, a differential gear set, two axle shafts, and two tires. For simplicity, each shaft is represented by two inertial elements connected by a spring element. The model is similar to those in Refs. [21–23]. The reduction gear set has a ring and a pinion. The number of rings and pinion teeth determines the reduction gear ratio. Its model includes the inertia of the ring and pinion, as well as the lash and gear tooth stiffness, similar to Ref. [20].

The vehicle is assumed to be a rigid body with a lumped mass because its dynamics do not contribute to the vehicle performance. We assume no slip between the tire and the road. The driveline parameters have less effect on clunk compared with the engine torque on the driveline [14,15]. There is no study to our knowledge that has considered optimizing the engine torque input to reduce clunk using engine torque management. When engine torque management is applied, the net torque on the driveline is relatively low. In this case, the variation in lash and friction becomes important and is included in this study.

The driveline system has many points where lash and friction are present. Every component interface has a finite amount of lash, and every bearing produces a finite amount of friction. The largest contribution to system lash is the ring and pinion in the rear axle with a nominal of approximately 7 deg. All other driveline components have a smaller than 0.5 deg lash. Because the ring and pinion of the rear axle have much more lash than any other driveline component, its variation has a dominant effect and must be considered. A random parameter L_{RP} (lash at the ring and pinion) is used in this study to account for the lash at the ring and pinion.

Friction is also important in driveline clunk. All bearings and the viscous fluid contribute to friction. The viscous friction is caused by the gear lubrication. The driveline friction is modeled as a lump sum parameter. The axle friction varies due to wear and temperature. As the vehicle is first built, the axle bearings are tight. After the vehicle break-in period, the bearings wear slightly, resulting in less friction. In addition to bearing wear, temperature also affects driveline friction. Because there is lube in the ring gear, the friction is purely viscous. When the gear lube heats up, the fluid viscosity is reduced, reducing friction. In this article, a random parameter R_{ring} accounts for the friction variation due to temperature and wear.

4 Time-Dependent Metamodels Using Principal Component Analysis

A variety of metamodeling techniques have been developed over the years and have been used in design. Metamodels are

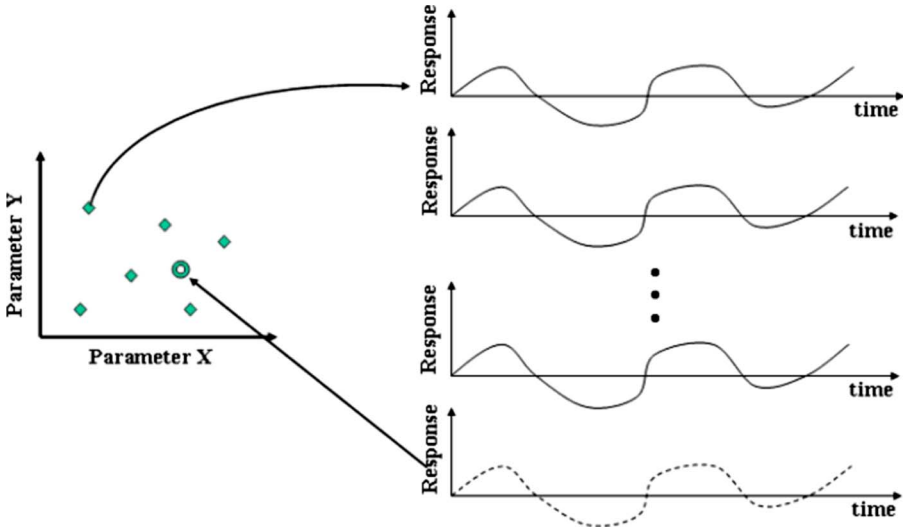

Fig. 4 Illustration of parametric case

computationally efficient "surrogates" of expensive simulations or experiments. Among the commonly used methods are polynomial response surfaces, kriging models, radial basis functions, moving least-squares, multivariate adaptive regression splines, artificial neural network methods, and multistage Bayesian surrogates.

Kriging is an interpolation technique originally developed in geostatistics [25]. It considers the true function $y(x)$ as a realization of a random process $Y(x)=f(x)+Z(x)$, where $f(x)$ is a deterministic regression model, and $Z(x)$ is a random error, which is represented by a zero-mean stochastic Gaussian process [26] with covariance $\mathrm{COV}(x_1,x_2)=\sigma^2 R(x_1,x_2)$, where σ^2 is the process variance and $R(x_1,x_2)$ is the correlation function. The Gaussian correlation function is common, although other multiple correlation functions exist [27]. Kriging is a widely used nonparametric interpolator with good capabilities in capturing nonlinear local behavior in contrast to parametric interpolators such as polynomial response surfaces. A good overview of metamodeling techniques including kriging, their use in design, and relevant sampling strategies for computer experiments can be found in Refs. [28–30].

A multistage Bayesian surrogate methodology (MBSM) has been also proposed [31–33]. It creates surrogate models using a Bayesian framework. The models are updated sequentially through multiple stages of refinements based on targeted data collection. MBSM has a lot of similarities with kriging. It provides however, a systematic and computationally efficient way to create and update surrogate models using information from different sources, such as simulations, experiments, expert opinion, or heuristics.

Kriging and all previously mentioned metamodeling methods are time independent. They simply provide a scalar estimate of the true function $y(x)$ at point x, which is different from a set of training points (design) used to build the metamodel. It is common however, in practice, to have time-dependent functions, which may represent the response of dynamic systems for example. To our knowledge, only the MBSM technique has been extended to time-dependent problems [34,35]. Our proposed methodology is an extension of Ref. [36]. It has also similarities with a recently reported method [37], which extracts the main features of a random field in the form of eigenvectors of its correlation matrix, using proper orthogonal decomposition, which in principle is similar to the Karhunen–Loeve (KL) decomposition [38].

This section gives a brief overview of a time-dependent metamodeling technique using singular value decomposition (SVD) [39] and kriging [25–30]. The method uses concepts from the principal component analysis. It first characterizes a parametric random process using an available finite number of time-dependent sample functions. Subsequently, it can "sample" the random process, producing time-dependent sample functions, which belong to the same random process. Both a parametric case in Sec. 4.1 and a nonparametric case in Sec. 4.2 are considered. The parametric case of the time-dependent metamodeling has been also used in Refs. [36,40].

4.1 Parametric Case. In this case, the random process is defined by a number of random variables. A realization of all random variables, defines a time-dependent sample function of the random process. The harmonic random process $A\sin(\omega t)$ is an example, where the magnitude A and the frequency ω are random variables.

Figure 4 illustrates the parametric uncertainty for a two-random variable case. For each sample of the input random variables, the output is a time-dependent sample function of the output random process.

We assume that the random process can be fully characterized using m sample functions. Each sample function corresponds to a particular design (sample point of input random variables). A $m \times n$ response matrix, $[X]$, is formed by discretizing each of the m output sample functions in time, using n time increments. Each row of the response matrix represents the discretized time history for a particular design (see Eq. (1)). Each column corresponds to a particular time step. The time-dependent metamodel of this section can provide the time history of a new design (circle in Fig. 4), which is not represented by any row of matrix $[X]$. Without loss of generality, we assume that $m \leq n$ resulting in $r \leq m$, where r is the rank of matrix $[X]$, where

$$[X] = \begin{bmatrix} x_1(t_1) & \cdots & x_1(t_n) \\ \vdots & \ddots & \vdots \\ x_m(t_1) & \cdots & x_m(t_1) \end{bmatrix} \tag{1}$$

The time histories in $[X]$ contain all potential nonlinear effects. The methodology can be therefore, applied to both linear and nonlinear systems. A SVD is performed on matrix $[X]$ according to the following relation [39]:

$$[X] = [U][S][V]^T \tag{2}$$

$[U]$ is a column-orthogonal $m \times m$ matrix, with each column being the left eigenvector of $[X]$, $[V]^T$ is an orthogonal $n \times n$ matrix

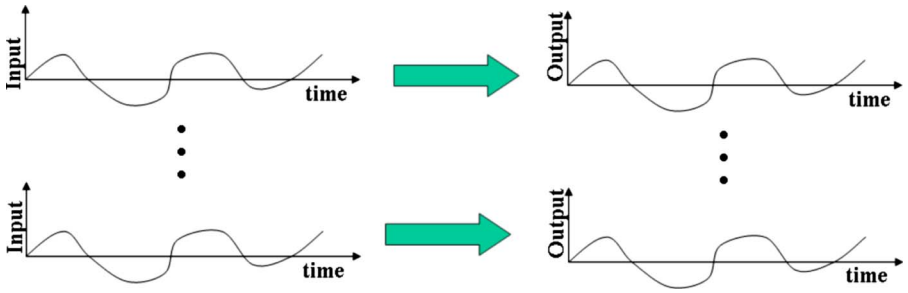

Fig. 5 Illustration of nonparametric case

of the right eigenvectors of $[X]$, and $[S]$ is an $m \times n$ matrix containing all m singular values of $[X]$ in decreasing magnitude in its upper diagonal portion. The matrix $[V]^T$ includes all time-dependent information of $[X]$, and matrices $[U]$ and $[S]$ are time-independent.

Keeping only the dominant singular values in $[S]$, Eq. (2) is partitioned as

$$[X] = \begin{bmatrix} M_\nu & M \end{bmatrix} \begin{bmatrix} S_\upsilon & 0 \\ 0 & 0 \end{bmatrix} \begin{bmatrix} P_\nu^T \\ P^T \end{bmatrix} \tag{3}$$

where the diagonal matrix S_ν includes the ν dominant singular values. The remaining $m-\nu$ nondominant singular values are truncated to zero. The columns of $[U]$ are called principal components and can be viewed as space-dependent "modes" of $[X]$. Finally, Eq. (3) becomes

$$[X] = [M_\nu][S_\upsilon][P_\nu]^T \tag{4}$$

Each row of matrix $[X]$ represents the time history for a particular sample design point. To characterize the random process, a number of design points equal to m were used to "space-fill" the design space. An optimum symmetric Latin hypercube (OSLH) sampling algorithm [41] is used to define the m design points. The time-dependent response $\{X(k)\}$ of a design point k, which is not included in the m sample design points, is calculated using a nonlinear interpolation of each "mode" of matrix $[M_\nu]$ in Eq. (4) as

$$\{X(k)\} = \{M_\upsilon(k)\}[S_\upsilon][P_\nu]^T \tag{5}$$

$\{X(k)\}$ is an "interpolated" row of the response matrix, corresponding to design point k, where $\{M_\upsilon(k)\}$ is an interpolated row of matrix $[M_\nu]$. The time-dependent information in matrix $[P_\nu]$ remains the same. We use kriging to calculate $\{M_\upsilon(k)\}$ because it provides an accurate interpolation for nonlinear functions. It uses a spatial correlation function so that the prediction is heavily influenced by sample points close to the prediction point. This feature greatly improves the interpolation accuracy.

The software package Design and Analysis of Computer Experiments (DACE) [27], a MATLAB toolbox, is used to create all kriging metamodels. A zero-order regression model and a Gaussian correlation function are used.

4.2 Nonparametric Case. For the nonparametric case, the input random process is an ensemble of time-dependent sample functions, as shown in Fig. 5. A response time function corresponds to each input sample function, as indicated by the arrows. All response time functions constitute the output random process.

Each time function of the input random process is discretized in time, and an input response matrix $[X_{\text{in}}]$ is formed similarly to Eq. (1). According to Eq. (2), a singular value decomposition results in $[X_{\text{in}}]=[U_{\text{in}}][S_{\text{in}}][V_{\text{in}}]^T$ or in a least-squares sense,

$$[U_{\text{in}}] = [X_{\text{in}}][V_{\text{in}}][S_{\text{in}}]^{-1} \tag{6}$$

where $[S_{\text{in}}]$ is the diagonal matrix of the ν dominant singular values. Similarly for the output random process, we have

$$[U_{\text{out}}] = [X_{\text{out}}][V_{\text{out}}][S_{\text{out}}]^{-1} \tag{7}$$

where $[X_{\text{out}}]$ is the response matrix of the output random process. At this point, a kriging interpolation is established between $[U_{\text{in}}]$ and $[U_{\text{out}}]$. For a given input time function $\{X_{\text{in}}^k(t)\} = \{X_{\text{in}}^k(t_1) \ldots X_{\text{in}}^k(t_n)\}$, which is discretized in time, we calculate $\{U_{\text{in}}^k\} = \{U_{\text{in}_1}^k \ldots U_{\text{in}_\nu}^k\}$ using Eq. (6), i.e.,

$$\{U_{\text{in}}^k\} = \{X_{\text{in}}^k\}[V_{\text{in}}][S_{\text{in}}]^{-1} \tag{8}$$

Using the kriging interpolation, which is established between $[U_{\text{in}}]$ and $[U_{\text{out}}]$, the output vector $\{U_{\text{out}}^k\}$ is calculated. Finally, the output time function, which corresponds to $\{X_{\text{in}}^k(t)\}$ is given by

$$\{X_{\text{out}}^k\} = \{U_{\text{out}}^k\}[S_{\text{out}}][V_{\text{out}}]^T \tag{9}$$

5 Time-Dependent Metamodels for Engine Torque and Turbine Speed

This section describes how time-dependent metamodels of a nonparametric case (see Sec. 4.2) are used to interpolate an existing set of functions comprising the engine torque random process and the corresponding turbine speed functions. The engine torque random process is first sampled, and the corresponding turbine speed is then calculated without running the actual simulation model. The process described herein is utilized in the deterministic optimization in Sec. 6.

A torsional full vehicle model of a rear-wheel-drive light duty truck is considered. A set of engine torque time histories (input) and the corresponding turbine speed time histories (output) are used to create an input-output relationship between engine torque and turbine speed.

Figure 6 shows the 25 input engine torque sample functions. They cover the entire range of possible engine torque functions. All engine torque time histories have similar shapes according to commonly used engine torque profiles in the automotive industry. With the exception of the baseline, each history is broken into two distinct regions. The first region represents the torque management phase, where the engine torque is controlled. The engine torque rises gradually until the lash is closed. In the second phase, the engine torque is unmanaged, jumping suddenly to the driver's requested torque. For the function with no torque management, the engine torque rises very quickly, early in time. The gradual torque rise of all functions except the baseline helps to reduce clunk.

For each input engine torque time function, the corresponding transmission turbine speed time function is calculated using the analytical model in Sec. 3. Figure 7 shows the calculated turbine speeds. Some of the time histories have a peak spike early in time and some later. The time at which the spike occurs indicates when the driveline lash is closed.

Using the process in Sec. 4.2, the 25 sample functions in Figs. 6 and 7 were used to characterize the input engine torque and the

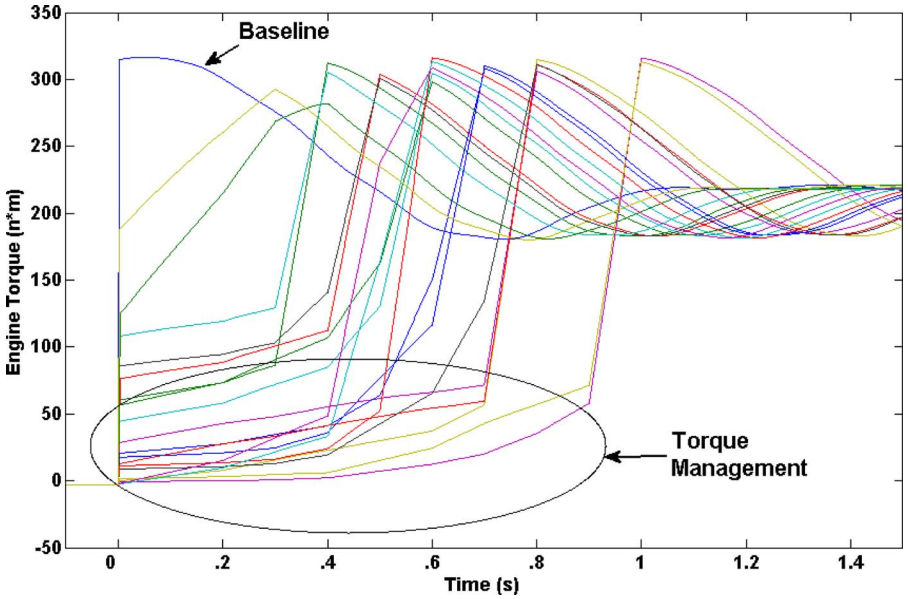

Fig. 6 Engine torque sample functions

output turbine speed random processes, respectively. According to Eq. (9), an interpolated engine torque function and its corresponding turbine speed function are given by

$$\{X_e\} = \{U_e\}[S_e][V_e]^T \tag{10}$$

and

$$\{X_t\} = \{U_t\}[S_t][V_t]^T \tag{11}$$

where the subscripts e and t indicate engine and transmission, respectively.

The number of kept singular values in Eqs. (10) and (11) was increased until the rms error (see Eq. (12)), between the predicted time function and the time function from the actual simulation, was less than 1 N m and 5 rpm, respectively. 10 and 12 singular values were needed for the input engine torque and the output turbine speed, respectively. Therefore, the dimensions of matrices $[U_e]$ and $[U_t]$ (see Eqs. (6) and (7)) are 25×10 and 25×12, respectively. Using kriging interpolation, we can predict the row of the output matrix $[U_t]$, which corresponds to an interpolated row of the input matrix $[U_e]$ as follows.

An integer number from 1 to n is assigned to each of the n rows of the $n\times m$ matrix $[U_e]$. A kriging interpolation model is then created between a real "counter" x with $1\leq x\leq n$, and the matrix of $[U_e]$. For each noninteger value of x we get an interpolated row $\{U_e^x\}=\{U_{e_1}^x \ldots U_{e_m}^x\}$ of $[U_e]$. If x is an integer, we simply obtain the original xth row of $[U_e]$. The xth row $\{U_t^x\}=\{U_{t_1}^x \ldots U_{t_m}^x\}$ of the output matrix $[U_t]$ is similarly obtained. Finally using Eqs. (10) and (11), the actual time functions $\{X_e^x\}=\{U_e^x\}[S_e][V_e]^T$ and $\{X_t^x\}=\{U_t^x\}[S_t][V_t]^T$ are calculated. This process is used to interpolate the 25 input engine torque functions in Fig. 6 and the corresponding 25 output turbine speed functions in Fig. 7.

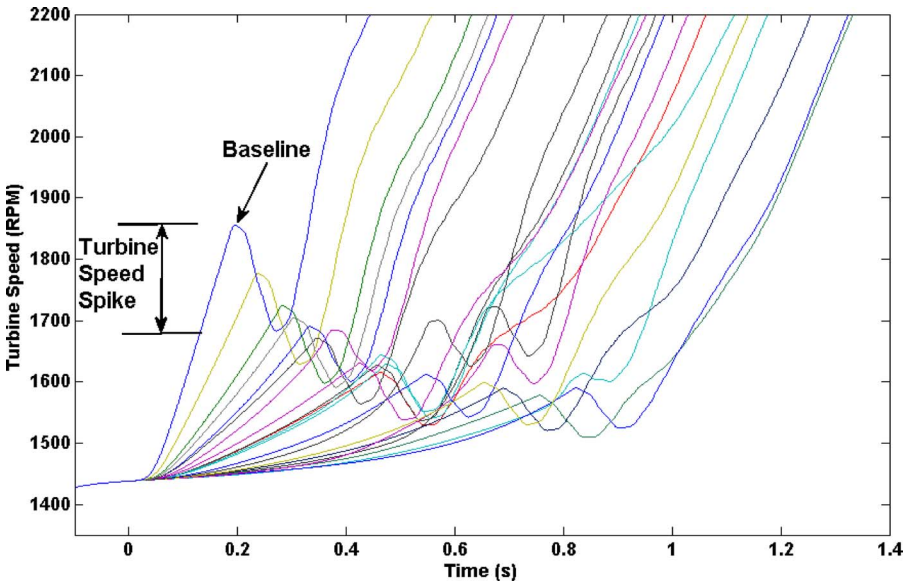

Fig. 7 Corresponding transmission turbine speed sample functions

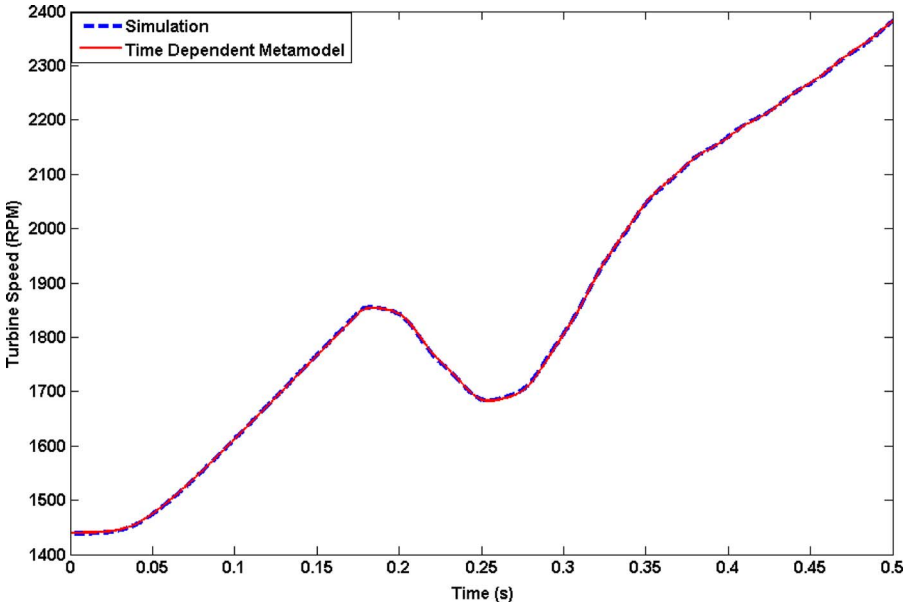

Fig. 8 Illustration of time-dependent metamodel validation

The accuracy of the time-dependent metamodels and the required number of time functions to build them were assessed using a "leave-one-out" approach. A time function is left out at a time, and a metamodel is built using the remaining functions. Subsequently, the metamodel is used to predict the left out function and an rms error is calculated using Eq. (12). We kept adding functions until the average rms error was less than 5 rpm. Twenty five functions were needed for the metamodel in the deterministic optimization of Sec. 6, and 100 functions were needed for the reliability-based design optimization (RBDO) metamodel in Sec. 7.

The rms error

$$E_{\text{rms}} = \sqrt{\frac{\sum_{i=1}^{n} (x_i - \hat{x}_i)^2}{n}} \tag{12}$$

is calculated using the difference between the function value x_i of the actual simulation and the function value $\hat{x}_i$ of the time-dependent metamodel at all discrete times $i=1,2,\ldots,n$. A time step of 0.001 s is used. Figure 8 compares a value predicted by the metamodel time function with the actual function for the deterministic optimization case, after the leave-one-out approach indicated that 25 functions are needed. The two functions are visually identical, indicating that the rms error of 5 rpm is relatively small.

6 Deterministic Optimization of Engine Torque During a Tip-In Event

The optimal engine torque profile is determined here without considering variation, providing a basis of comparison when variation is considered in Sec. 7. In practice, engine calibration is performed using manual iterations, based on subjective feedback provided by experienced calibration engineers. In calibration for tip-in clunk, the calibration engineer enters an aggressive engine torque profile if the throttle response is too slow, and a slower engine torque rate if the clunk event is perceived as too objectionable. A production calibration is achieved when both the throttle response and the clunk magnitude are perceived as acceptable. This article provides an analytical methodology for improved engine calibration for clunk, using objective (not subjective) measures, optimization, and time-dependent metamodels.

Using time-dependent metamodels, the turbine speed can be predicted for any engine torque input as a function of time without running the actual simulation model. It has been mentioned that the rate of engine torque rise affects the vehicle response time significantly, and that a trade-off exists between reduced clunk disturbance and vehicle performance. An optimization is therefore, used to reduce clunk while maintaining an acceptable level of vehicle performance.

The following deterministic optimization problem is solved:

$$\min_{x}[f(x,\mathbf{p})]$$

$$\text{s.t.} \quad G(x,\mathbf{p}) \leq 0.67$$

$$1 \leq x \leq 25 \tag{13}$$

where the objective $f(x,\mathbf{p})$ represents the magnitude of the turbine speed spike during a tip-in event. Because the spike is proportional to the clunk severity, minimizing $f(x,\mathbf{p})$ also minimizes clunk. In Eq. (13), the design variable x provides an interpolation counter among the engine torque profiles and the corresponding turbine speeds (see last paragraph of Sec. 5). Vector $\mathbf{p}$ includes the deterministic parameters. The constraint $G(x,\mathbf{p})$ represents the vehicle throttle response. It ensures that clunk is reduced without causing excessive throttle delays due to torque management. It also measures how quickly the vehicle reacts to throttle pedal movement. Both $f(x,\mathbf{p})$ and $G(x,\mathbf{p})$ are determined from postprocessing the turbine speed time trace.

During tip-in, the engine torque should only be "managed" while the driveline is traveling through the lash zone. The engine torque can, subsequently, rise rapidly without producing clunk. In this article, an acceptable throttle response is defined by the time it takes the engine torque to rise to 150 N m, because the clunk event is over by the time the engine is producing 150 N m. The upper limit for the throttle response constraint $G(x,\mathbf{p})$ is equal to 0.67 s (see Fig. 9), which is representative of a rear-wheel-drive light duty truck. This constraint is essential for the trade-off between throttle response (vehicle performance) and clunk reduction.

Figure 9 shows the deterministically optimal engine torque from Eq. (13) and the baseline design with no engine torque management. The latter indicates, as expected, a sharp initial rise in the engine torque. The optimal engine torque exhibits a gradual slope to allow the lash to close without accelerating the gear sets. Also the throttle response constraint $G(x,\mathbf{p}) \leq 0.67$ is active.

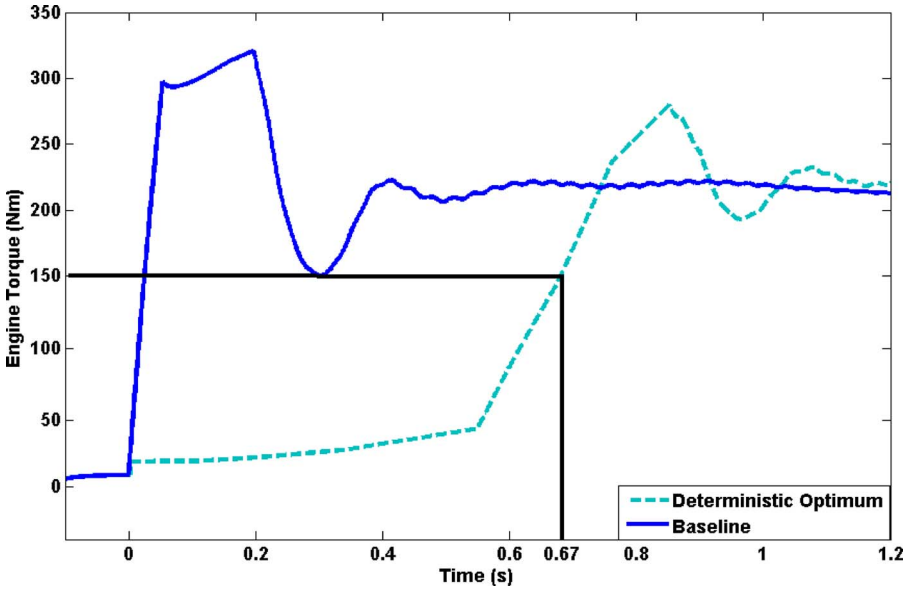

Fig. 9 Initial and optimal engine torques

The baseline and optimal torque functions were used as inputs to the time-dependent metamodel, and the corresponding turbine speed outputs in Fig. 10 were obtained. The baseline turbine speed experiences a relatively high turbine speed spike of 166 rpm, indicating a high level of clunk. The result is expected because there is no torque management to slow the driveline acceleration while in the lash zone. The turbine speed however, which corresponds to the deterministically optimal engine torque, has a much lower turbine speed spike of 65 rpm, resulting in a much lower level of clunk. For comparison purposes, the optimal turbine speed from the reliability-based design optimization study in Sec. 7 is also shown.

7 Reliability-Based Design Optimization of Engine Torque

The optimization in Sec. 6 was performed without considering the inherent variation in a vehicle population. As mentioned in Sec. 3, variation exists in the engine, torque converter, and driveline. The engine and torque converter variation is represented by the positive scalar multiplication factors ETV, TRV, and KFV. The driveline variability is characterized by L_{RP} (lash at the ring and pinion) and R_{ring} (friction variation due to temperature and wear). The ETV, KFV, and TRV design parameters are assumed to follow a truncated normal distribution $N(0.975, 0.05)$, so that they vary between 0.95 and 1. The R_{ring} and L_{RP} design parameters are assumed normally distributed with $R_{ring} \sim N(0.2, 0.02)$, and $L_{RP} \sim N(0.275, 0.02)$

Based on available but limited data, ETV, KFV, and TRV are close to, but smaller than, 1, and their COV is around 5%. Also the COV for R_{ring} and L_{RP} is around 10%. Due to lack of further information, we assumed normal distributions with approximately, the above COVs. We believe that because our goal is to demonstrate the effect of uncertainty in the design of vehicle drivelines with reduced clunk, the assumed normal distributions are reasonable. More work is needed to assess the input distributions using limited available data.

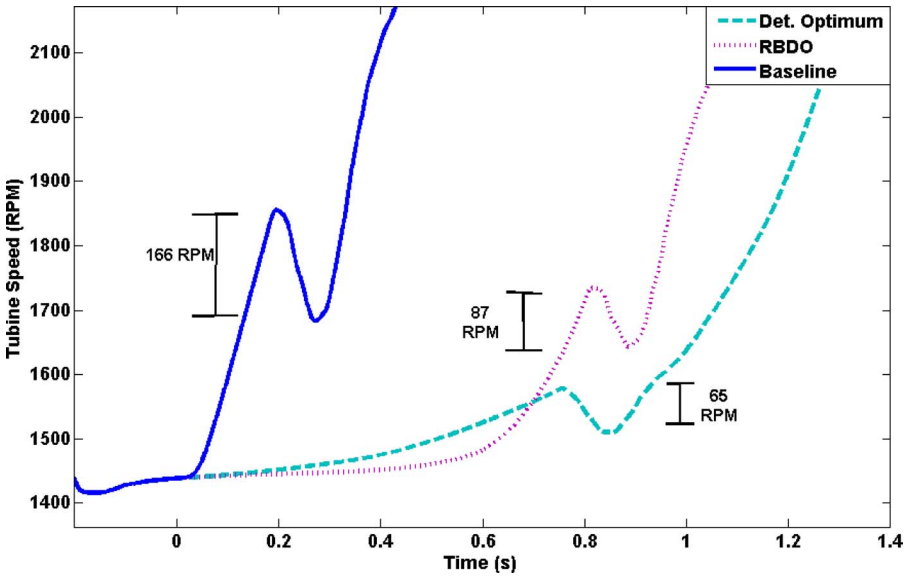

Fig. 10 Initial and optimal turbine speed functions

Table 1 Input sample space for the RBDO case

Point	Counter x	ETV	KFV	TRV	L_{RP}	R_{ring}
1	1.000	0.950	0.950	0.950	0.250	0.100
2	25.000	1.000	1.000	1.000	0.300	0.300
3	13.606	0.972	0.951	0.981	0.289	0.209
4	5.848	0.984	0.984	0.952	0.289	0.153
5	20.152	0.966	0.966	0.998	0.261	0.247
6	8.273	0.955	0.967	0.963	0.299	0.172
7	17.727	0.995	0.983	0.987	0.251	0.228
8	12.394	0.978	0.999	0.969	0.261	0.191
9	24.515	0.985	0.972	0.987	0.280	0.173
10	1.485	0.965	0.978	0.963	0.270	0.227
…						
99	20.394	0.956	0.953	0.988	0.255	0.165
100	5.606	0.994	0.997	0.962	0.295	0.235

The input sample space is now six-dimensional (the interpolation counter x for the engine torque and five random parameters ETV, TRV, KFV, L_{RP}, and R_{ring}). As mentioned in Sec. 5, we used a leave-one-out approach to determine the number of input design points so that the average rms error is less than 5 rpm. One hundred points were needed. Points were created using the "space filling" OSLH design in six dimensions. Table 1 shows some of the OSLH design points. The counter x is used to interpolate the engine torque random process according to Sec. 4.1. The calculated engine torque time function and the values of the ETV, TRV, KFV, L_{RP}, and R_{ring} random parameters are used as inputs in the actual simulation model of Sec. 3 to calculate the corresponding turbine speed time function. The engine torque and turbine speed time functions are postprocessed to obtain the throttle response $G(x,\mathbf{p})$ and the turbine speed spike $f(x,\mathbf{p})$, respectively.

The optimal engine torque profile under uncertainty is calculated by solving the following RBDO problem

$$\min_{d}[f(d,\boldsymbol{\mu}_{\mathbf{P}},\mathbf{p})]$$

$$P(G(d,\mathbf{P},\mathbf{p}) \le 0) \ge R$$

$$1 \le d \le 100 \tag{14}$$

where d is a new counter for interpolation among the engine torque profiles and the corresponding turbine speeds of the 100 OSLH design points (first column of Table 1). The vectors $\boldsymbol{\mu}_{\mathbf{p}}$ =[0.975 0.975 0.975 0.275 0.2] and $\boldsymbol{\sigma}_{\mathbf{p}}$ =[0.05 0.05 0.05 0.015 0.02] represent the mean and standard deviation values of the random parameters $\mathbf{P}$ =[ETV KFV TRV L_{RP} R_{ring}], and the vector $\mathbf{p}$ includes all deterministic parameters. In the deterministic optimization in Sec. 6, the mean values of L_{RP} and R_{ring} have been used, and the parameters ETV, KFV, and TRV are equal to 1. The desired reliability level is denoted by $R=1-p_f$ where $p_f=P(G(d,\mathbf{P})>0)$ is the target probability of violating the throttle response constraint. We have assumed that $p_f \approx \Phi(-\beta)$ where the target reliability index β is equal to 2. The RBDO problem of Eq. (14) is solved using the single-loop RBDO algorithm of Liang et al. [42].

Figure 11 shows the optimal engine torque from RBDO in comparison with the deterministic optimal engine torque. The former rises slightly more gradually because of the presence of variation. Both curves look similar and exhibit the peak torque at nearly the same time. However, they are controlled slightly differently ear-

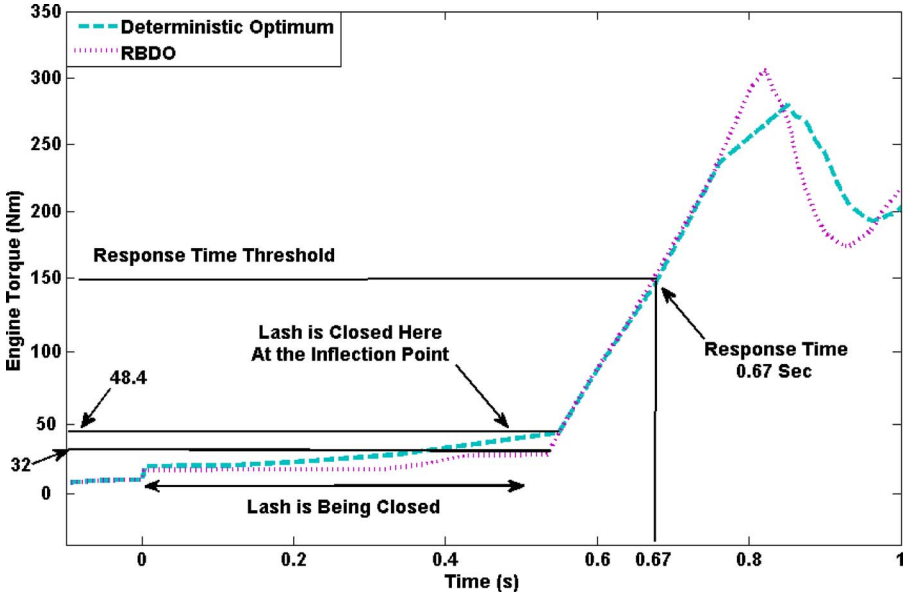

Fig. 11 Optimal engine torque functions

lier in time, when the engine torque is less than 50 N m, until the lash is closed. This is indicated by the different slope and the different inflection point as the engine torque transitions from managed to unmanaged. The lash is closed when the engine torque reaches 48.4 N m in the deterministic case, and 32 N m in the RBDO case. The important portion of the engine torque between 0 N m and 50 N m depends on the vehicle application.

Figure 10 shows the resulting turbine speeds for the engine torques in Fig. 11. The presence of variation resulted in a 34% increase in clunk, increasing the turbine speed spike from 65 rpm to 87 rpm. Small changes in the engine torque management, or variation in the driveline, can have, therefore, a large impact on clunk. For a fleet of vehicles, the engine torque management and the driveline must be simultaneously optimized under uncertainty.

8 Summary, Conclusions, and Future Work

A methodology has been proposed to create time-dependent metamodels for parametric and nonparametric cases using principal component analysis and kriging. The methodology was used to optimize the engine torque profile under uncertainty for a rear-wheel-drive light duty truck in order to reduce the driveline tip-in clunk disturbance without greatly affecting the vehicle performance. Driveline clunk negatively affects the perceived quality and must be minimized. This is usually achieved using engine torque management, which is part of engine calibration. The proposed technique can replace the time consuming and relatively inaccurate current practice of trial-and-error engine calibration, which uses the subjective judgment of the calibration engineer(s). It was shown that the turbine speed spike, which serves as a driveline clunk measure, is reduced from 166 rpm at the baseline design to 87 rpm for the optimum design under uncertainty. The required engine torque to reduce the level of clunk resulted in a longer throttle response and therefore, a lower vehicle performance. The lost performance however, was small and acceptable considering the substantial clunk reduction.

It was demonstrated that small changes in engine torque management, or variation in the driveline, can have a large impact on the level of clunk. This suggests that the engine torque and the driveline design must be simultaneously optimized under uncertainty, in order to minimize clunk for a fleet of vehicles.

In this article, clunk was optimized deterministically and also under uncertainty using engine torque management at the expense of throttle response. Based on our findings, the following two recommendations for future work are proposed.

There is a trade-off between clunk reduction and throttle response. The latter indicates vehicle performance. In this article, clunk was minimized under the assumption of the throttle response not exceeding a target of 0.67 s. Although this target is acceptable in light duty truck design, a multi-objective optimization should be considered in which the clunk and the throttle response are simultaneously minimized. The resulting Pareto front will better guide the designer in choosing the appropriate compromise between cluck and vehicle performance.

The development of "learning" algorithms to automatically modify the engine torque during the vehicle life will be very useful. As the vehicle ages, the engine torque compression ratio decreases, causing the engine to produce less torque. In this article, we only accounted for the variation in engine torque among different engines. However, we did not consider the engine torque reduction during the life of the vehicle, which is expected to be sizeable. An algorithm can detect clunk using the turbine speed spike, and can adjust the engine torque management to reduce clunk and to also reduce the delay in the perceived throttle response. The techniques in Refs. [1–3] can be incorporated into the design of such an algorithm.

Acknowledgment

General Motors Corporation has provided financial support for the first author's studies at Oakland University. The support is gratefully acknowledged.

References

[1] Langerberg, A., and Egardt, B. S., 2002, "Evaluation of Control Strategies for Automotive Powertrains With Backlash," International Symposium on Advanced Vehicle Control, Hiroshima, Japan.

[2] Lagerberg, A., and Egardt, B. S., 2005, "Model Predictive Control of Automotive Powertrains With Backlash," *Proceedings of the IFAC World Congress*, Prague, Czech Republic.

[3] Lagerberg, A., and Egardt, B. S., 2007, "Backlash Estimation With Application to Automotive Powertrains," IEEE Trans. Control Syst. Technol., **15**(3), pp. 483–493.

[4] Millo, F., Ferraro, C. V., Mallamo, F., and Pilo, L., 2003, "Numerical Simulation to Improve Engine Control During Tip-In Manoeuvres," SAE Paper No. 2003-01-0374.

[5] Theodossiades, S., Gnanakumarr, M., and Rahnejat, H., 2005, "Root Cause Identification and Physics of Impact-Induced Driveline Noise in Vehicular Powertrain Systems," Proc. Inst. Mech. Eng., Part D (J. Automob. Eng.), **219**, (11), pp. 1303–1319.

[6] Govindswamy, K., Hueser, M., D'Anna, T., Diemer, P., and Roxin, C., 2003, "Study of Low-Frequency Driveline Clunk During Static Engagements," SAE Paper No. 2003-01-1480.

[7] Volinski, B., 1999, "Automatic Transaxle Lash Study for Park Disengagement Clunk," SAE Paper No. 1999-01-1765.

[8] Chae, C., Lee, Y., Won, K., and Kang, K., 2004, "Experimental and Analytical Approach for Identification of Driveline Clunk Source and Transfer Path," SAE Paper No. 2004-01-1231.

[9] Biermann, J. W., and Hagerodt, B., 1999, "Investigation of the Clonk Phenomenon in Vehicle Transmissions: Measurement, Modeling and Simulation," Proc. Inst. Mech. Eng., Part K: J. Multi-Body Dynamics, **213**(1), pp. 53–60.

[10] Vafaei, S., Menday, M., and Rahnejat, H., 2001, "Transient High-Frequency Elasto-Acoustic Response of a Vehicular Drivetrain to Sudden Throttle Demand," Proc. Inst. Mech. Eng., Part K: J. Multi-Body Dynamics, **215**(1), pp. 35–52.

[11] Theodossiades, S., Gnanakumarr, M., Rahnejat, H., and Menday, M., 2004, "Mode Identification in Impact-Induced High-frequency Vehicular Driveline Vibrations Using an Elasto-Multi-Body Dynamics Approach," Proc. Inst. Mech. Eng., Part K: J. Multi-Body Dynamics, **218**(2), pp. 81–94.

[12] Menday, M. T., Rahnejat, H., and Ebrahimi, M., 1999, "Clonk an Onomatopoeic Response in Torsional Impact of Automotive Drivelines," Int. J. Mech. Eng. Educ., **213**(4), pp. 349–357.

[13] Gnanakumarr, M., Theodossiades, S., Rahnejat, H., and Menday, M., 2005, "Impact-induced Vibration in Vehicular Driveline Systems: Theoretical and Experimental Investigations," Proc. Inst. Mech. Eng., Part K: J. Multi-Body Dynamics, **219**(1), pp. 1–12.

[14] Oh, W., and Singh, R., 2005, "Examination of Clunk Phenomena Using a Non-Linear Torsional Model of a Front-Wheel-Drive Vehicle With Manual Transmission," Proceedings of the SAE, Paper No. 2005-01-2291.

[15] Schumacher, T., Biermann, J. W., Jansz, N., Willey, J., and Küpper, K., 2003, "Load Change Reactions of Passenger Cars: Method of Investigation and Improvement," Proc. Inst. Mech. Eng., Part K: J. Multi-Body Dynamics, **217**(4), pp. 283–291.

[16] Krentz, R. A., 1985, "Vehicle Response to Throttle Tip-In/Tip Out," SAE Paper No. 850967.

[17] Crowther, A. R., Zhang, N., and Singh, R., 2005, "Development of a Clunk Simulation Model for a Rear-Wheel-Drive Vehicle With Automatic Transmission," SAE Paper No. 2005-01-2292.

[18] Gilbert, D. A., O'Leary, M. F., and Rayce, J. A., 2001, "Integrating Test and Analytical Methods for the Quantification and Identification of Manual Transmission Driveline Clunk," SAE Paper No. 2001-01-1502.

[19] Couderc, P., Callenaere, J., Der Hagopian, J., Ferraris, G., Kassai, A., Borjesson, Y., Verdillon, L., and Gaimard, S., 1998, "Vehicle Driveline Dynamic Behaviour: Experimentation and Simulation," J. Sound Vib., **218**(1), pp. 133–157.

[20] Karnopp, D. C., Margolis, D. L., and Rosenberg, R. C., 2000, *System Dynamics*, Wiley, New York.

[21] Louca, L. S., Stein, J. L., and Geoff, R. D., 2001, "Generating Proper Integrated Dynamic Models for Vehicle Mobility Using a Bond Graph Formulation," *Proceedings of the International Conference on Bond Graph Modeling*, Phoenix, AZ, Vol. 33, pp. 339–345.

[22] Karnopp, D. C., 1976, "Bond Graphs for Vehicle Dynamics," Veh. Syst. Dyn., **5**, pp. 171–184.

[23] Wehrwein, D., and Mourelatos, Z. P., 2008, "Reliability-Based Design Optimization of Vehicle Drivetrain Dynamic Vehicle Performance," Int. J. Prod. Dev., **5**(1/2), pp. 54–75.

[24] Kim, H. M., Kokkolaras, M., Louca, L. S., Delagrammatikas, G. J., Michelena, N. F., Filipi, Z. S., Papalambros, P. Y., Stein, J. L., and Assanis, D. N., 2002, "Target Cascading in Vehicle Redesign: A Class VI Truck Study," Int. J. Veh. Des., **29**(3), pp. 199–225.

[25] Cressie, N., 1993, *Statistics for Spatial Data*, Wiley, New York.

[26] Sacks, J., Welch, W. J., Mitchell, J. J., and Wynn, H. P., 1989, "Design and

Analysis of Computer Experiments," Stat. Sci., **4**(4), pp. 409–435.
[27] Lophaven, S. N., Nielsen, H. B., and Sondergaard, J., 2002, "DACE: A MATLAB Kriging ToolBox," Technical Report No. IMM-TR-2002-12.
[28] Wang, G. G., and Shan, S., 2007, "Review of Metamodeling Techniques in Support of Engineering Design Optimization," ASME J. Mech. Des., **129**(4), pp. 370–380.
[29] Simpson, T. W., Peplinski, J. D., Koch, P. N., and Allen, J. K., 2001, "Metamodels for Computer-Based Engineering Design: Survey and Recommendations," Eng. Comput., **17**(2), pp. 129–150.
[30] Simpson, T. W., Lin, D. K. J., and Chen, W., 2001, "Sampling Strategies for Computer Experiments: Design and Analysis," Int. J. Reliab. Appl., **2**(3), pp. 209–240.
[31] Pacheco, J. E., Amon, C. H., and Finger, S., 2003, "Bayesian Surrogates Applied to Conceptual Stages of the Engineering Design Process," ASME J. Mech. Des., **125**, pp. 664–672.
[32] Weiss, L. E., Amon, C. H., Finger, S., Miller, E. D., Romero, D., Verdinelli, I., Walker, L. M., and Campbell, P. G., 2005, "Bayesian Computer-Aided Experimental Design of Heterogeneous Scaffolds for Tissue Engineering," Comput.-Aided Des., **37**, pp. 1127–1139.
[33] Romero, D. A., Amon, C. H., and Finger, S., 2006, "On Adaptive Sampling for Single and Multi-Response Bayesian Surrogate Models," ASME Paper No. DETC2006-99210.
[34] Romero, D. A., Amon, C. H., and Finger, S., 2003, "Modeling Time-Dependent Systems Using Multi-Stage Bayesian Surrogates," ASME Paper No. IMECE2003-55049.
[35] Romero, D. A., Amon, C. H., Finger, S., and Verdinelli, I., 2004, "Multi-Stage Bayesian Surrogates for the Design of Time-Dependent Systems," ASMEPaper No. DETC2004-57510.
[36] Sun, J., and Vlahopoulos, N., 2005, "Model Update Under Uncertainty and Error Estimation in Shock Applications," SAE Paper No. 2005-01-2373.
[37] Missoum, S., 2008, "Probabilistic Optimal Design in the Presence of Random Fields," Struct. Multidiscip. Optim., **35**, pp. 523–530.
[38] Ghanem, R., and Spanos, P. D., 1991, *Stochastic Finite Elements: A Spectral Approach*, Springer, New York.
[39] Strang, G., 1998, *Introduction to Linear Algebra*, Wellesley-Cambridge, Wellesley, MA.
[40] Wehrwein, D., and Mourelatos, Z. P., 2007, "Optimal Engine Torque Management for Reducing Driveline Clunk Using Time-Dependent Metamodels," SAE Paper No. 2007-01-2236.
[41] Ye, K. Q., Li, W., and Sundjianto, A., 2000, "Algorithmic Construction of Optimal Symmetric Latin Hypercube Designs," J. Stat. Plan. Infer., **90**, pp. 145–159.
[42] Liang, J., Mourelatos, Z. P., and Tu, J., 2008, "A Single-Loop Method for Reliability-Based Design Optimization," Int. J. Prod. Dev., **5**(1/2), pp. 76–92.